


Controllable Microparticle Spinning via Light without Spin Angular MomentumYi-Jing Wu¹,[✉] Pan-Pan Yu,¹ Yi-Fan Liu,¹ Jing-Han Zhuang,¹ Zi-Qiang Wang,¹ Yin-Mei Li,^{1,2}
Cheng-Wei Qiu,^{3,*} and Lei Gong^{1,2,†}¹*Department of Optics and Optical Engineering, University of Science and Technology of China, Hefei 230026, China*²*Hefei National Research Center for Physical Sciences at the Microscale,
University of Science and Technology of China, Hefei, China*³*Department of Electrical and Computer Engineering, National University of Singapore, Singapore, Singapore* (Received 6 January 2024; accepted 20 May 2024; published 21 June 2024)

The spin angular momentum (SAM) of an elliptically or circularly polarized light beam can be transferred to matter to drive a spinning motion. It is counterintuitive to find that a light beam without SAM can also cause the spinning of microparticles. Here, we demonstrate controllable spinning of birefringent microparticles via a tightly focused radially polarized vortex beam that has no SAM prior to focusing. To this end, the orbital Hall effect is proposed to control the radial separation of two spin components in the focused field, and tunable transfer of local SAM to microparticles is achieved by manipulating the twisted wavefront of the source light. Our work broadens the perspectives for controllable exertion of optical torques via the spin-orbit interactions.

DOI: [10.1103/PhysRevLett.132.253803](https://doi.org/10.1103/PhysRevLett.132.253803)

Introduction.—The light-matter interaction is governed by the conservation laws of energy, momentum and angular momentum [1–3]. Like energy and momentum, optical angular momentum (AM) is also a fundamental dynamic property of light, including spin angular momentum (SAM) and orbital angular momentum (OAM) [4]. The SAM is associated with the polarization helicity and usually carried by elliptically or circularly polarized (CP) light waves [5]. OAM has two parts: intrinsic OAM and extrinsic OAM. The former is characterized by twisted helical wavefronts [6], while the latter is related to the trajectory of light [7]. The intrinsic OAM of light, similar to the SAM, has a handedness based on a clockwise or anticlockwise twist, and the topological charge is used to characterize the vorticity of twisted light. The transfer of AM from light to matter can generate optical torques at the microscale, which has been employed for mechanical applications such as micropumps and optical manipulations [8–11]. Rubinsztein-Dunlop *et al.* first confirmed the AM transfer by rotating a particle in an optical tweezer [12,13]. Miles Padgett *et al.* later revealed that the SAM transfer produced a rotation of the particle around its own axis (i.e., optical spinning), and the transfer of OAM resulted in orbital motion around the beam axis [14]. People commonly use CP light for optical spinning, but it remains challenging to spin multiple particles and control their spinning independently.

SAM and OAM of light often couple with each other through a process known as spin-orbit interaction (SOI) [15–17]. A fundamental manifestation of SOI, the optical spin-Hall effect (SHE), occurs in inhomogeneous media, at optical interfaces, or in free-space nonparaxial fields [18–20]. Actually, there also exist interactions between the

intrinsic OAM and extrinsic OAM, for example, the orbital-Hall effect (OHE) [17,21,22]. Particularly, the SOI can be harnessed to tailor one AM by manipulating the other, offering a way to control the transfer of AM. For instance, the CP light focused by a high numerical aperture (NA) lens generates a helicity-dependent vortex, termed spin-to-orbital AM conversion [23–26]. Because of the helicity-dependent OAM transfer, microparticles experience orbital rotation with the direction determined by the helicity of the incoming light [24]. This kind of conversion can be interpreted as an azimuthal SHE in cylindrically symmetric fields [27,28]. Recent studies show that the OAM of light can also influence the SAM distribution in the focused light, termed vorticity-dependent SAM [29–31], which has been studied in cylindrical vector vortex beams [30], linearly polarized vortex beams [31], higher-order Poincaré sphere beams [25], and self-torqued beams [32]. However, existing studies recognized that there was no change in the total amount of SAM before and after focusing [29–32], but local SAM arose under tight focusing even the source light had no SAM. The physics underlying this phenomenon has not been revealed and it is unknown whether light without SAM can exert optical torques to spin microparticles.

Here, we present a physical interpretation of the vorticity-dependent SAM under tight focusing via the optical SHE and OHE. Under this physical framework, we harness the optical OHE to manipulate the vorticity-dependent separation of two spin components in the focal field and enhance the local SAM density. Further, we achieve switchable microparticle spinning via source light without SAM by controlling the transfer of local SAM to optically trapped microparticles. Direct evidence is captured by

reversible spinning of a birefringent microparticle using a radially polarized vortex beam (RPVB). Dynamic switching of the spinning directions of two trapped particles is also achieved by manipulating the twisted wavefront of incident light. Our work reveals that twisted light can also be used to spin a particle around its own axis, which offers a way for controllable exertion of optical torques. The physical mechanism provides insights for both SOI and optical rotation, and the mechanical manifestations are expected to benefit applications such as optofluidics and optical manipulations.

Theory.—To understand the origin of the vorticity-dependent SAM, we note that focusing with a high-NA lens rotates the wave vector of the incoming collimated beam in the meridional planes and thus generates a conical k distribution in the focused field (Fig. 1). The focused field is described by the Richards-Wolf approach, where any vector field can be represented by a linear combination of radially and azimuthally polarized fields [33]. To simplify the discussion, we analyze a RPVB that retains its local vectors in the transverse plane after focusing. The electric field of a RPVB with topological charge l_0 can be expressed as

$$\begin{aligned} E(\rho, \varphi) &\propto A(\rho) \exp(il_0\varphi) (\cos\varphi \hat{x} + \sin\varphi \hat{y}) \\ &= A(\rho) \exp(il_0\varphi) \left(\exp(i\varphi) \frac{\hat{x} - i\hat{y}}{2} + \exp(-i\varphi) \frac{\hat{x} + i\hat{y}}{2} \right) \\ &= |\sigma = -1, l = l_0 + 1\rangle + |\sigma = 1, l = l_0 - 1\rangle, \end{aligned} \quad (1)$$

where $A(\rho)$ represents the cylindrically symmetric amplitude and (ρ, φ) are the polar coordinates of the incident plane. The equation suggests that the RPVB can be

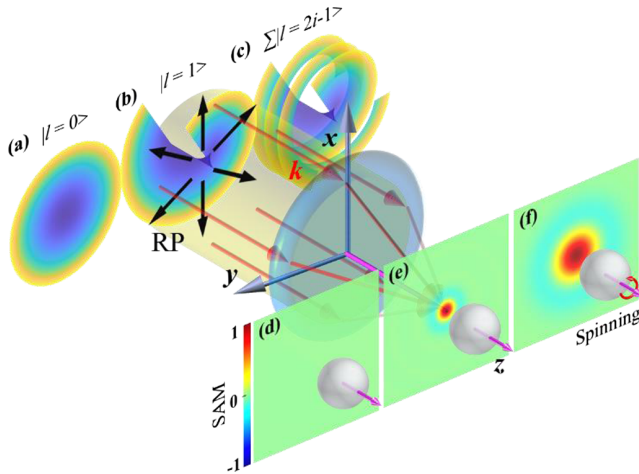


FIG. 1. Illustration of controllable microparticle spinning via a source light without SAM by the transfer of local SAM under focusing. (a)–(c) Twisted wavefronts of the radially polarized (RP) field for tunable SAM transfer, characterized by the topological charge l . $\sum_i |l = 2i - 1| = |l = 1| + |l = 3| + |l = 5| + \dots$. (d)–(f) Corresponding SAM density distributions in the focal plane.

described as a superposition of left-handed and right-handed circularly polarized components (helicity $\sigma = \pm 1$) of equal amplitude. Thus, the RPVBs carry no SAM. Upon tight focusing in free space, the optical Hall effect occurs, including the SHE and the OHE, causing a subwavelength transverse shift for both components. Specifically, this transverse shift in the focal plane, depending on the helicity σ and the vorticity l of the source light, can be expressed as [17,22]

$$\Delta \mathbf{r} = \frac{l + (1 - \cos\theta)\sigma}{\sin\theta k_0} \hat{\boldsymbol{\phi}}, \quad (2)$$

where θ is the polar angle on the output pupil of the focused system with $\sin\theta_{\max} = \text{NA}$, and k_0 is the wave number of light. $\hat{\boldsymbol{\phi}} = -\sin\varphi \hat{x} + \cos\varphi \hat{y}$ describes the local azimuthal unit vector. For each CP component with cylindrically symmetric amplitude $A(\rho)$, the intensity of the focal beam exhibits a ring profile with the radius given by

$$r = \int_0^{\theta_{\max}} \Delta r A^2(\rho) P^2(\theta) \sin\theta d\theta \triangleq l r_l + \sigma r_\sigma, \quad (3)$$

where $P(\theta) = \sqrt{\cos\theta}$ is the apodization function of the focusing system. $r_l = \int_0^{\theta_{\max}} A^2(\rho) P^2(\theta) / k_0 d\theta$ and $r_\sigma = \int_0^{\theta_{\max}} (1 - \cos\theta) A^2(\rho) P^2(\theta) / k_0 d\theta$ are the contributions to the beam shift from the OHE and the SHE, respectively. Considering $r_l \gg r_\sigma$, the beam shifts due to the SHE upon tight focusing can be ignored, and thus, $r \simeq l r_l$.

Such an optical Hall effect can be used to explain the origin of the vorticity-dependent SAM in focused light. When the incident field has no OAM ($l_0 = 0$), the transverse shifts for the two CP components with opposite helicities will be exactly the same, $|r_L| = |r_R|$. Thus, there is no separation between the two beam components in the focal plane [Figs. 1(a) and 1(d)]. In contrast, when the incident field has an OAM ($l_0 \neq 0$), the corresponding transverse shifts will be different, leading to a vorticity-dependent separation in the focal plane [Figs. 1(b) and 1(e)]. Actually, the focal field presents two distinct rings of helicity with opposite signs. Quantitatively, the separation between the two rings can be calculated via Eq. (3), which equals

$$|r_R| - |r_L| = 2 \text{sign}(l_0) r_l. \quad (4)$$

It is a subwavelength separation, and the focal field is inhomogeneous at the wavelength scale. Under such circumstances, particles that interact with the focal field will experience differential light-matter interactions depending on their size and handedness. However, it is difficult to predict the motion of particles of several wavelengths in size due to the complicated position-dependent average effect.

To address this problem, we propose a strategy to break the separation limit given by Eq. (4) by means of the OHE. For a RPVB with a single OAM eigenstate represented by Eq. (1), the separation between the two spin components is independent of the magnitude of l_0 . In contrast, when the RPVB holds an OAM superposition state, the separation can be l -dependent. For this purpose, we construct a RPVB with a designed superposition OAM state, which reads

$$\begin{aligned} E &= (|\sigma = -1, l = 1\rangle + |\sigma = 1, l = -1\rangle) \\ &\quad (|l = 1\rangle + |l = 3\rangle + |l = 5\rangle + \dots) \\ &= |\sigma = 1, l = 0\rangle + |\sigma = 1, l = 2\rangle + |\sigma = 1, l = 4\rangle + \dots \\ &\quad + |\sigma = -1, l = 2\rangle + |\sigma = -1, l = 4\rangle + |\sigma = -1, l = 6\rangle + \dots \\ &= |\sigma = 1, l = 0\rangle + |\sigma = 0, l = 2\rangle + \dots + |\sigma = -1, l = 2n\rangle. \end{aligned} \quad (5)$$

The superposition OAM state can be expressed as $\sum_{i=1}^n |l = 2i - 1\rangle$, and $n \geq 1$ is defined as the enhancement factor. In this case, the separation between the two rings of opposite helicity $\sigma = \pm 1$ will be

$$|r_R| - |r_L| = 2nr_l. \quad (6)$$

Actually, this equation applies to any integer n . If $n \leq -1$, it corresponds to the superposition state of $\sum_{i=1}^{-n} |l = -2i + 1\rangle$. In this case, the helicity of the two rings reverses. For the case of $n = 0$, the incident beam has no OAM. Remarkably, Eq. (6) suggests that the optical OHE can be used to manipulate the vorticity-dependent spin separation and enhance the local SAM density in the focused field. Therefore, controllable transfer of the local SAM to microparticles using RPVBs with superposition OAM states can be achieved [Figs. 1(c) and 1(f)].

Computation.—Following the proposed strategy, we perform numerical calculations to demonstrate the tunable separation between spin components in the focused field by regulating the twisted phase of incident light. It is worth noting that the superposition OAM state will lead to an interference effect and an inhomogeneous intensity distribution in the focused field. To obtain optimized intensity and SAM distributions in the focal plane, we design RPVBs with a multiring twisted phase distribution, as illustrated in the insets of Figs. 2(a)–2(f). The multiring phase structure guarantees a uniform amplitude over the whole transverse plane and the same energy for each OAM component of the superposition state. Particularly, it can be directly generated by a phase-only spatial light modulator (SLM) used in the following experiment. Based on the designed wavefronts, we calculated the focal fields and the corresponding SAM density of the RPVBs using the vectorial Debye diffraction integral [34] with an NA of 0.92. In the calculation, we focus on the longitudinal SAM that plays a key role in the SAM transfer experiment.

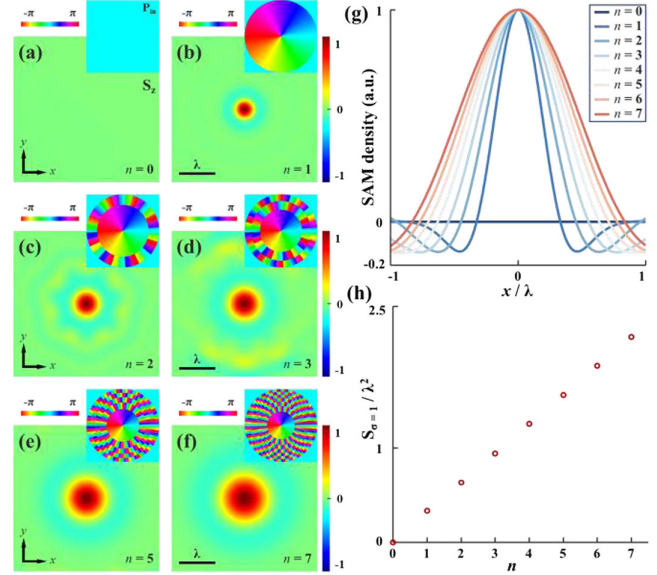


FIG. 2. Computational analysis of the tunable separation between spin components in the focused field by regulating the twisted phase of light. (a)–(f) Normalized longitudinal SAM distributions of various focused RPVBs for the case of $n = 0 \sim 7$. Inserts are the corresponding phase profiles of the RPVBs. (g) Plot of the x -axial distributions of the longitudinal SAM density. (h) Area of pure SAM of $\sigma = 1$ at the center versus the enhancement factor n .

Figure 2 shows the computation results of the longitudinal SAM density in the focal plane for various focused RPVBs. As a reference, the situation of an incident beam without OAM (i.e., $n = 0$) is presented in Fig. 2(a), and as expected, there is no SAM. In contrast, a longitudinal SAM appears upon tight focusing when the source light has a twisted wavefront, as demonstrated in Figs. 2(b)–2(f). For further examination, Fig. 2(g) plots the normalized distributions along the x axis of the longitudinal SAM density for various RPVBs represented by Eq. (5), i.e., $n = 0$ –7. The separation between the two beam components with opposite helicities can be tuned by the twisted phase of incident light. In particular, the area of the pure SAM ($\sigma = 1$) at the center of the focal plane expands with the increase of n , as shown in Fig. 2(h). The sign of the SAM can be reversed when an RPVB with $n < 0$ is adopted. These findings suggest that the local SAM density in the focal field can be manipulated and enhanced for tunable SAM transfer from a source light beam without SAM.

Experiment.—To test the SAM transfer, we employ an SLM (1920 \times 1080 pixels; PLUTO-2-VIS, Holoeye) and an S wave plate (Lithuania, Workshop of Photonics) to generate the desired RPVBs, which are tightly focused to trap and spin birefringent microparticles using holographic optical tweezers (HOT). A 532-nm laser (MSL-R-532-5W, Changchun New Industries) is used as the light source. A 20 \times beam expander enlarges the linearly polarized beam to fully illuminate the surface of the SLM. It modulates the

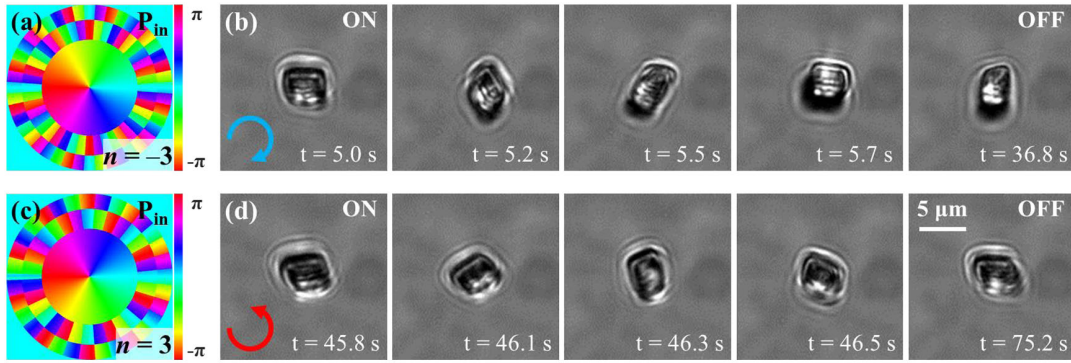


FIG. 3. Observation of the vorticity-dependent SAM transfer in a focused field via the reversible spin motion of a calcium carbonate particle. (a),(c) Phase masks projected to realize controlled rotation in opposite directions. (b),(d) Successive frames of the video recording the switchable rotation of a trapped microparticle. The circular arrows denote the spinning directions.

designed phase profiles, as shown in Figs. 3(a) and 3(c). Then, the S wave plate converts the linearly polarized field into the RPVB. The shaped field is relayed to the pupil plane of an objective lens ($100\times$, $NA = 1.3$; UPLFLN100XO2, Olympus). The HOT setup is built on an inverted microscope (IX73, Olympus), and real-time monitoring of the trapping and rotating process can be realized with the microscope and a CMOS camera (acA720-520um, Basler).

We demonstrated the tunable transfer of local SAM to birefringent microparticles from the RPVBs. A uniform phase and twisted phase were generated and switched by the SLM. A self-grounded calcium carbonate particle with a size of $\sim 5 \mu\text{m}$ was optically trapped, which did not spin when the uniform phase was projected. In contrast, when the twisted phase in Fig. 3(a) was switched at $t = 5.0 \text{ s}$, we observed a clockwise spinning of the trapped particle at a frequency of $\sim 0.8 \text{ Hz}$, as demonstrated in Fig. 3(b). Notably, the direction of the spinning can be switched by regulating the phase of incident field. When the twisted

phase in Fig. 3(c) for the case of $n = 3$ was projected at 45.8 s , as expected, the particle trapped by such a focused beam underwent spinning in a counterclockwise direction, as shown in Fig. 3(d). Video S1 shows the whole dynamic process of switchable rotations. These results conform with the computational analysis above and confirm the switchable SAM transfer from designed RPVBs to microparticles of several wavelengths in size. Furthermore, we find that the spin transfer rate in the optical trap can be modulated by tuning the enhancement factor n . Experimentally, the time-varying rotation speed of a trapped particle was realized and is demonstrated in Video S2. The rotation frequency is affected by both the spin density of the light and the particle itself, which is discussed in detail in the Supplemental Material [35].

It is worth noting that it is challenging for traditional HOT to achieve reversible spinning and translation of multiple particles because the phase and polarization of the optical field are mutually independent. Here, we exploit the proposed mechanism to control the translational and

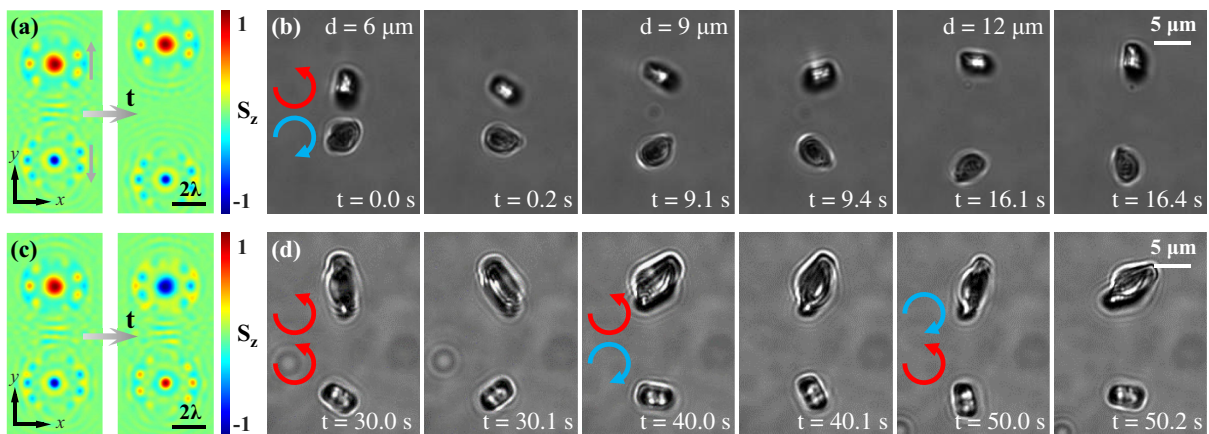


FIG. 4. Experimental demonstration of dynamic translational and rotational motions of microparticles. (a) Time-varying SAM distributions designed for dynamic translation of two particles spinning in opposite directions. (b) Typical frames that present the dynamic process of two particles spinning in opposite directions. The particles are moved in the transverse plane with a varying distance from $d = 6 \mu\text{m}$ to $d = 12 \mu\text{m}$. (c) SAM distributions designed for direction switching for the two-beam trap. (d) Typical frames that show switching of the directions. The circular arrows denote the spinning directions.

rotational motions simultaneously by regulating the twisted phase of light. First, we demonstrated the dynamic translation of two particles spinning in opposite directions. Figure 4(a) illustrates the time-varying SAM distributions in the focal plane corresponding to the RPVBs designed for dynamic manipulation, which can be used to predict the motion of the trapped particles. The motions were recorded in Video S3, where two $\sim 5\text{-}\mu\text{m}$ calcium carbonate particles were trapped with the focused beams and they rotated in the expected directions. In the meantime, we translated them individually to specific positions, as demonstrated in Fig. 4(b). What is more, we further demonstrated switching directions at will for the two-beam trap. Figure 4(c) plots the SAM distributions for the switching manipulation. The results are shown in Fig. 4(d) and Video S4, where the two spinning particles were made to dynamically switch directions. Conventionally, such a manipulation requires controlling the CP states of light. In contrast, our method requires shaping only the phase profile, and thus enhances the capability of HOT in optical rotation.

Conclusion.—In summary, we have revealed that the vorticity-dependent SAM upon tight focusing is a manifestation of the optical Hall effect. By exploiting the optical OHE, we are capable of manipulating the vorticity-dependent separation of two spin components in the focused RPVBs and enhancing the local SAM density. Furthermore, we demonstrate stable trapping and reversible spinning of birefringent microparticles by controlling the local SAM transfer to the particles. The experimental observations are well predicted by the theory. All the results confirm the controllable spinning of birefringent microparticles via light without SAM under tight focusing. Our work paves the way for the controllable exertion of optical torques via the SOI. It will benefit multidimensional optical tweezers with the ability of controlled rotation, translation, and optomechanical applications such as light-driven motors [8–11].

This work was supported by the National Natural Science Foundation of China (NSFC) under Grants No. 11974333 and No. 12204456, Anhui Natural Science Foundation (Grant No. 2208085J24) and Advanced Research and Technology Innovation Centre at the National University of Singapore (A-0005947-16-00).

*Corresponding author: eleqc@nus.edu.sg

†Corresponding author: leigong@ustc.edu.cn

- [1] A. Ashkin, *Phys. Rev. Lett.* **24**, 156 (1970).
- [2] A. Novitsky, C. W. Qiu, and H. F. Wang, *Phys. Rev. Lett.* **107** (2011).
- [3] A. Novitsky, C. W. Qiu, and A. Lavrinenko, *Phys. Rev. Lett.* **109** (2012).
- [4] K. Y. Bliokh and F. Nori, *Phys. Rep.* **592**, 1 (2015).
- [5] J. H. Poynting, *Proc. R. Soc. A* **82**, 560 (1909).

- [6] L. Allen, S. M. Barnett, and M. J. Padgett, *Optical Angular Momentum* (CRC Press, Boca Raton, 2016).
- [7] A. T. O’Neil, I. MacVicar, L. Allen, and M. J. Padgett, *Phys. Rev. Lett.* **88**, 053601 (2002).
- [8] I. D. Stoev, B. Seelbinder, E. Erben, N. Maghelli, and M. Kreysing, *eLight* **1** (2021).
- [9] Y. Z. Shi *et al.*, *Phys. Rev. Lett.* **129**, 053902 (2022).
- [10] A. Minopoli, S. Wagner, E. Erben, W. D. Liao, I. D. Stoev, E. Lauga, and M. Kreysing, *eLight* **3**, 16 (2023).
- [11] D. L. Gao, W. Q. Ding, M. Nieto-Vesperinas, X. M. Ding, M. Rahman, T. H. Zhang, C. Lim, and C. W. Qiu, *Light Sci. Appl.* **6**, e17039 (2017).
- [12] M. E. J. Friese, T. A. Nieminen, N. R. Heckenberg, and H. Rubinsztein-Dunlop, *Nature (London)* **394**, 348 (1998).
- [13] L. Paterson, M. P. MacDonald, J. Arlt, W. Sibbett, P. E. Bryant, and K. Dholakia, *Science* **292**, 912 (2001).
- [14] M. Padgett and R. Bowman, *Nat. Photonics* **5**, 343 (2011).
- [15] O. Hosten and P. Kwiat, *Science* **319**, 787 (2008).
- [16] S. S. Zhang, Z. Y. Zhou, Y. A. Fu, Q. Chen, W. P. Li, H. Fang, C. J. Min, Y. Q. Zhang, and X. C. Yuan, *Opt. Express* **31**, 5820 (2023).
- [17] K. Y. Bliokh, F. J. Rodriguez-Fortuno, F. Nori, and A. V. Zayats, *Nat. Photonics* **9**, 796 (2015).
- [18] A. Aiello, N. Lindlein, C. Marquardt, and G. Leuchs, *Phys. Rev. Lett.* **103**, 100401 (2009).
- [19] X. H. Ling, X. X. Zhou, K. Huang, Y. C. Liu, C. W. Qiu, H. L. Luo, and S. C. Wen, *Rep. Prog. Phys.* **80**, 066401 (2017).
- [20] W. X. Shu, C. Y. Lin, J. Wu, S. Z. Chen, X. H. Ling, X. X. Zhou, H. L. Luo, and S. C. Wen, *Phys. Rev. A* **101**, 023819 (2020).
- [21] M. Merano, N. Hermosa, J. P. Woerdman, and A. Aiello, *Phys. Rev. A* **82**, 023817 (2010).
- [22] K. Y. Bliokh, M. A. Alonso, E. A. Ostrovskaya, and A. Aiello, *Phys. Rev. A* **82**, 063825 (2010).
- [23] Y. Q. Zhao, J. S. Edgar, G. D. M. Jeffries, D. McGloin, and D. T. Chiu, *Phys. Rev. Lett.* **99**, 073901 (2007).
- [24] Y. Q. Zhao, D. Shapiro, D. McGloin, D. T. Chiu, and S. Marchesini, *Opt. Express* **17**, 23316 (2009).
- [25] P. P. Yu, Y. F. Liu, Z. Q. Wang, Y. M. Li, and L. Gong, *Ann. Phys. (Amsterdam)* **532**, 2000110 (2020).
- [26] K. Y. Bliokh, E. A. Ostrovskaya, M. A. Alonso, O. G. Rodriguez-Herrera, D. Lara, and C. Dainty, *Opt. Express* **19**, 26132 (2011).
- [27] Z. Bomzon and M. Gu, *Opt. Lett.* **32**, 3017 (2007).
- [28] D. Haefner, S. Sukhov, and A. Dogariu, *Phys. Rev. Lett.* **102**, 123903 (2009).
- [29] L. Han, S. Liu, P. Li, Y. Zhang, H. C. Cheng, and J. L. Zhao, *Phys. Rev. A* **97**, 053802 (2018).
- [30] P. Shi, L. P. Du, and X. C. Yuan, *Opt. Express* **26**, 23449 (2018).
- [31] P. P. Yu, Q. Zhao, X. Y. Hu, Y. M. Li, and L. Gong, *Opt. Lett.* **43**, 5677 (2018).
- [32] Y. J. Wu, P. P. Yu, Y. F. Liu, Z. Q. Wang, Y. M. Li, and L. Gong, *J. Lightwave Technol.* **41**, 2252 (2023).
- [33] B. Richards and E. Wolf, *Proc. R. Soc. A* **253**, 358 (1959).
- [34] Y. Hu, Z. Wang, X. Wang, S. Ji, C. Zhang, J. Li, W. Zhu, D. Wu, and J. Chu, *Light Sci. Appl.* **9**, 119 (2020).
- [35] See Supplemental Material at <http://link.aps.org/supplemental/10.1103/PhysRevLett.132.253803> for a detailed discussion of the influence factors of the spin transfer rate.